Springer

Journal of
Mechanical
Science and
Technology

Journal of Mechanical Science and Technology 22 (2008) 1586~1601

www.springerlink.com/content/1738-494x
DOI 10.1007/s12206-008-0431-8

Supercritical droplet dynamics and emission in low speed cross-flows

J. W. Chae[1], H. S. Yang[2] and W. S. Yoon[2,*]

[1]*Korea Aerospace Research Institute (KARI), Daejeon, Korea 305-333*
[2]*Department of Mechanical Engineering, Yonsei University, Seoul, Korea 120-749*

(Manuscript Received December 11, 2007; Revised April 15, 2008; Accepted April 28, 2008)

Abstract

Droplet dynamics and emission of a supercritical droplet in crossing gas stream are numerically investigated. Effects of ambient pressure and velocity of nitrogen gas on the dynamics of the supercritical oxygen droplet are parametrically examined. Unsteady conservative axisymmetric Navier-Stokes equations. in curvilinear coordinates are preconditioned and solved by dual-time stepping method. A unified property evaluation scheme based on a fundamental equation of state and extended corresponding-state principle is established to deal with thermodynamic non-idealities and transport anomalies.

At lower pressures and velocities of nitrogen cross flows, both the diffusion and the convection are important in determining the droplet dynamics. Relative flow motion causes a secondary breakup and cascading vortices, and the droplet lifetime is reduced with increasing in ambient pressure. At higher ambient pressures and velocities, however, the droplet dynamics become convection-controlled while the secondary breakup is hindered by reduced diffusivity of the oxygen. Gas-phase mixing depends on the convection and diffusion velocities in conjunction with corresponding droplet deformation and flow interaction. Supercritical droplet dynamics and emission is not similar with respect to the pressure and velocity of the ambient gas and thus provides no scale.

Keywords: Droplet dynamics; Supercritical emission; Cross flows; Fundamental equation of state; Droplet deformation; Secondary breakup

1. Introduction

Thermodynamic states inside the high-power engine combustor are typically supercritical to the liquid fuels including heavy hydrocarbons (up to $C_{20}H_n$) [1, 2]. A droplet initially exposed to supercritical pressure, however, remains subcritical as it undergoes transcritical heating and eventually enters into the supercritical regime in which both the pressure and the temperature goes over its critical limit. This thermodynamic transient of the droplet is featured by thermodynamic non-idealities and transport anomalies [3]; as the liquid at droplet surface reaches at its critical locus, densities of gas and liquid phases are equalized at the gas-liquid interface, and this interfacial boundary becomes no longer descriptive. Unlike the subcritical droplet vaporization, the characteristic times of the transport processes in both phases have the same order of magnitude, and unsteady effects in the gas phase becomes as important as those in the liquid phase. The process never reaches a quasi-steady state up to the termination of the droplet evolution [4], and thus classical models incorporated with the quasi-steady approximation fail in this limit. Hubbard et al. [5] demonstrated that the quasi-steady assumption results in small error if the ambient pressure is below 10 bar (≈10 atm); however it is invalid for high-pressure applications. The quasi-steady theory may not be well practiced for the thermodynamic state with reduced pressure greater than 0.1 [6].

As droplet exceeds its critical mixing state, it essentially becomes a puff of dense fluid, which is a continuous medium, and a sharp distinction of interfacial

*Corresponding author. Tel.: +82 2 2123 4812, Fax.: +82 2 312 2159
E-mail address: wsyoon@yonsei.ac.kr

boundary between gas and liquid phases disappears. Near the critical point, the mixture poses liquid-like densities and gas-like diffusivities, and pressure-dependent solubility. The solubility effects, which are typically negligible at low pressures, become essential considerations at high pressures. Surface tension and enthalpy of vaporization approach zero, and isothermal compressibility and specific heat increase significantly. These critical thermophysical effects coupled with extreme local property variations, have a significant impact on the evolutionary dynamics [7, 8]. In addition, their collective effect elongates the droplet transient processes significantly, and makes the quasi-steady approximation at low pressures invalid. The entire process is diffusion-controlled by dense supercritical fluid rather than the droplet vaporization [9, 10, 11].

A number of experimental, mathematical, and computational studies on droplet vaporization and combustion have been carried out extensively for diverse industrial applications [12]. Earlier studies adopted certain rudimentary assumptions and empirical formulas for fluid properties that were extrapolated from low-pressure cases, with their accuracy for high-pressure applications subject to question. Accordingly, a series of fundamental studies were conducted using state-of-the-art treatment of thermodynamic and transport phenomena to treat the thermodynamic phase transition through the critical point. Of particular importance are the unified analyses of thermophysical properties based on fundamental thermodynamic theories. These approaches allow for a self-consistent solution from the first principles, thereby enabling a systematic investigation into underlying mechanisms involved in supercritical droplet gasification and combustion. Hsieh et al. [7] developed a theoretical-numerical method to investigate multi-component droplet vaporization at near critical conditions. Time-dependent conservation equations. for fluids are solved for droplet dynamics with a full account of variable properties and vapor-liquid interfacial thermodynamics. This analysis comprehends various high-pressure phenomena, i.e. ambient gas solubility, property variation, thermodynamic non-ideality, and transient diffusion. Shuen et al. [8] extended this model and numerically investigated the gasification and the burning mechanism of fuel-droplet in both sub- and supercritical environments [13]. They showed that, the vaporization of liquid fuel dominates the burning characteristics of the droplet at subcritical pressures, whereas the transient diffusion of gas phase at the supercritical pressures. Hsiao [14] studied the gasification of isolated oxygen (LOX) in a hydrogen stream over a range of ambient pressure (100-400 atm) and Reynolds number (20-300), and showed that the forced convection has a great deal of influence on droplet dynamics and gasification characteristics.

The present study targets a comprehensive modeling of high-pressure emission and secondary breakup of a droplet in cross flow. Strongly conservative flow equations. incorporated with a local preconditioning method solve the dynamics of the droplet and carrier fluids. Comprehensive fluid models treat thermophysical properties at high pressure. Solution strategy repeats that adopted in previous theoretical-numerical studies by Hsieh et al. [7], Shuen et al. [8], and Hsiao [14] but with emphasis laid on the rigorous property evaluation scheme based on the fundamental equation of state. Effects of the ambient pressure and the cross-flow velocity on the supercritical droplet dynamics are parametrically investigated.

2. Modeling of a supercritical droplet dynamics

A physical model of interest is an isolated liquid-like oxygen droplet suddenly introduced into a strongly convective nitrogen gas stream (Fig. 1). Initial droplet temperature is assumed to be subcritical and uniform. Since the temperature and the pressure of the nitrogen carrier gas are above the critical values of the oxygen, subcritical oxygen droplet progressively transits to the supercritical state. Then, with regard to cryogenic properties of the oxygen, they are in a puff state. The puff-state density of the oxygen is close to liquid density and hence this supercritical fluid is frequently called as “liquid-like gas”. When

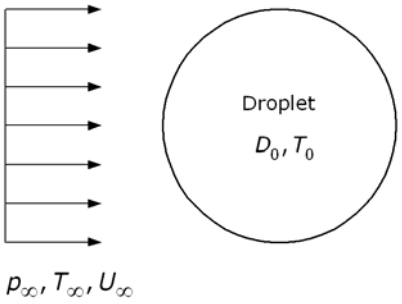

Fig. 1. A schematic diagram of droplet exposed to a crossing gas stream.

the droplet is at the puff state, enthalpy of vaporization and surface tension vanish and the dynamics of the supercritical droplet evolving in the cross gas stream is approximated by that of the gas mixture.

2.1 Formulation and numerical strategy

Dynamics of evolving supercritical droplet in crossing gas stream is well approximated by the axisymmetric laminar flow. If body forces and thermal radiation are ignored, the conservation laws of mass, axial and radial momentum, energy, and species concentration can be written in the following conservative form of equations.

$$\frac{\partial r\rho}{\partial t}+\frac{\partial r\rho u}{\partial x}+\frac{\partial r\rho v}{\partial r}=0 \tag{1}$$

$$\frac{\partial r\rho u}{\partial t}+\frac{\partial}{\partial x}\left[r\left(\rho u^2+p\right)\right]+\frac{\partial r\rho uv}{\partial r}=\frac{\partial r\tau_{xx}}{\partial x}+\frac{\partial r\tau_{rx}}{\partial r} \tag{2}$$

$$\frac{\partial r\rho v}{\partial t}+\frac{\partial r\rho uv}{\partial x}+\frac{\partial}{\partial r}\left[r\left(\rho v^2+p\right)\right]=\frac{\partial r\tau_{xr}}{\partial x}+\frac{\partial r\tau_{rr}}{\partial r}+p-\tau_{\theta\theta} \tag{3}$$

$$\frac{\partial r\rho e_t}{\partial t}+\frac{\partial}{\partial x}\left[ru\left(\rho e_t+p\right)\right]+\frac{\partial}{\partial r}\left[rv\left(\rho e_t+p\right)\right]=\frac{\partial}{\partial x}\left(ru\tau_{xx}\right)+\frac{\partial}{\partial r}\left(ru\tau_{rx}\right)+\frac{\partial}{\partial x}\left(rv\tau_{xr}\right)+\frac{\partial}{\partial r}\left(rv\tau_{rr}\right)-\frac{\partial r\left(q_e\right)_x}{\partial x}-\frac{\partial r\left(q_e\right)_r}{\partial r} \tag{4}$$

$$\frac{\partial r\rho Y_i}{\partial t}+\frac{\partial r\rho uY_i}{\partial x}+\frac{\partial r\rho vY_i}{\partial r}=-\frac{\partial r\left(q_{m,i}\right)_x}{\partial x}-\frac{\partial r\left(q_{m,i}\right)_r}{\partial r} \tag{5}$$

The physical variables t, u, v, and Y_i are time, axial and radial velocities, and mass fraction of species i, respectively. e_t is the specific total internal energy, and τ_{xx}, τ_{rr}, and $\tau_{\theta\theta}$ are the normal stresses and τ_{xr}, τ_{rx} are the shear stresses.

$$\tau_{xx}=\mu\left[2\frac{\partial u}{\partial x}-\frac{2}{3}\left(\frac{\partial u}{\partial x}+\frac{1}{r}\frac{\partial}{\partial r}\left(rv\right)\right)\right]$$

$$\tau_{rr}=\mu\left[2\frac{\partial v}{\partial x}-\frac{2}{3}\left(\frac{\partial u}{\partial x}+\frac{1}{r}\frac{\partial}{\partial r}\left(rv\right)\right)\right]$$

$$\tau_{\theta\theta}=\mu\left[2\frac{v}{r}-\frac{2}{3}\left(\frac{\partial u}{\partial x}+\frac{1}{r}\frac{\partial}{\partial r}\left(rv\right)\right)\right]$$

$$\tau_{xr}=\tau_{rx}=\mu\left(\frac{\partial u}{\partial r}+\frac{\partial v}{\partial x}\right)$$

μ is the dynamic viscosity, and thermal $\left(q_e\right)$ and species diffusion fluxes $\left(q_{m,i}\right)$ are related to the thermodynamic and flow variables by Fourier's and Fick's laws, respectively.

$$\left(q_e\right)_x=-\lambda\frac{\partial T}{\partial x}-\rho\sum_{i=1}^{N}h_iD_{im}\frac{\partial Y_i}{\partial x}$$

$$\left(q_e\right)_r=-\lambda\frac{\partial T}{\partial r}-\rho\sum_{i=1}^{N}h_iD_{im}\frac{\partial Y_i}{\partial r}$$

$$\left(q_{m,i}\right)_x=-\rho D_{im}\frac{\partial Y_i}{\partial x}$$

$$\left(q_{m,i}\right)_r=-\rho D_{im}\frac{\partial Y_i}{\partial r}$$

T, λ, and D_{im} are temperature, thermal conductivity, and mass diffusivity for species i in the mixture, respectively.

The centerline boundary condition is easily implemented by exploiting axisymmetry of the flowfield. Normal velocity and gradients of the pressure, axial velocity, temperature, and species concentration must be zero for symmetry.

$$v\big|_{r=0}=0 \tag{6}$$

$$\frac{\partial p}{\partial r}\big|_{r=0}=\frac{\partial u}{\partial r}\big|_{r=0}=\frac{\partial T}{\partial r}\big|_{r=0}=\frac{\partial Y_i}{\partial r}\big|_{r=0}=0 \tag{7}$$

For subsonic inflow, the temperature, species concentration, axial and radial velocities are specified. Pressure is extrapolated from the interior nodes. Since the flow is subsonic throughout entire flowfield, the pressure is specified at the outlet boundary, whereas other flow variables are extrapolated from the interior nodes.

Droplet vaporization in cross flows incorporates fluid motions in a velocity range from molecular diffusion to low subsonic speed. Contemporary numerical algorithms developed for compressible flows are often ineffective for such low Mach flows. There are two well-recognized reasons for this difficulty [15]. First, the eigenvalues of the system become disparate at low flow velocities, thereby adversely affecting the convergence characteristics of numerical solutions. Secondly, the pressure-gradient term in the momentum equations. becomes singular as the Mach number

approximates to zero and causes a large round-off error. To circumvent such numerical difficulties, a fully implicit dual time-stepping integration method [13, 16] is adopted. The scheme is established in two steps. On one hand, rescaled pressure terms are used in the momentum equations. and minimize round-off errors expected at low Mach numbers. On the other hand, a set of well-conditioned artificial terms are incorporated into the conservation laws to enhance numerical efficiency and stability. An implicit iterative procedure follows to achieve a converged solution in the pseudo-time domain, which corresponds to temporal-accurate solution in the physical-time domain. One significant advantage of the dual time-stepping method is that the convergence of the iterative process is determined by the eigenvalues characteristics in the pseudo-time domain, and not by those in the physical domain; thus the numerical stiffness rarely hinders the convergence at physical time at low Mach numbers. This feature allows flexibility in determining the time step in both time frames. The physical time step is computed based on the characteristic evolution of the unsteady flow under consideration, while the pseudo-time step depends on the numerical stability of the algorithm and can be adjusted to obtain the optimum convergence [14].

2.2 Transport and thermodynamic properties

An equation of state is required to close the formulation for property evaluation. In the previous studies [14], Benedict-Webb-Rubin (BWR) equation of state is adopted. This cubic EOS is superior to other classical cubic equation of state (e.g., the SRK equation of state), but constants for this cubic EOS are valid only for a limited number of pure compounds. In order to mitigate this constraint, an extended corresponding-state (ECS) principle was used and the properties of a single-phase fluid was evaluated via conformal mappings of temperature and density to those of a given reference fluid. Only the BWR constants of the reference substance close the evaluation, and accuracy and applicable range of the conformed fluid depends on those reference fluids. If the reference fluid is properly chosen, the BWR equation of state in conjunction with the ECS principle yields good agreement with experimental data in a limited range. Basically, the use of BWR in combination with ECS principle is an indirect method and its availability is laid within a limited range and species.

To ensure the prediction accuracy and enlarge the availability range of EOS, a fundamental equation of state developed by Lemmon et al. [17, 18] is adopted in the present study. The term "fundamental equation" usually refers to equations containing calorimetric information so that the properties may be calculated directly by differentiation. This type of EOS requires additional information from ancillary equations for the isobaric heat capacity of ideal gas and datum states for the calculation of absolute values. Most practical fundamental EOS are explicit in Helmholtz energy and allow accurate calculation of thermodynamic properties such as density, energy, speed of sound, and heat capacities for pure fluids over a wide range of pressures and temperatures [17, 18]. The Helmholtz energy, a, can be expressed in a nondimensional form consisting of an ideal gas contribution, α^0, and a real fluid contribution, α^r.

$$\frac{a}{RT} = \alpha(\delta,\tau) = \alpha^0(\delta,\tau) + \alpha^r(\delta,\tau) \tag{8}$$

where $\delta = \rho/\rho_c$ and $\tau = T_c/T$.

The ideal gas contribution to the Helmholtz energy evaluated with isobaric heat capacity calculation yields the following simplified ideal gas Helmholtz energy [19],

$$\begin{aligned}\alpha^0 = {} & \ln\delta + a_1\ln\tau + a_2 + a_3\tau + a_4\tau^{-1} + a_5\tau^{-2} \\ & + a_6\tau^{-3} + a_7\ln\left[1-\exp\left(-a_8\tau\right)\right]\end{aligned} \tag{9}$$

The term α^r is the compressibility contribution to the dimensionless Helmholtz energy, and expressed for the nitrogen and oxygen as;

$$\begin{aligned}\alpha^r(\delta,\tau) = {} & \sum_{k=1}^{6} N_k\delta^{i_k}\tau^{j_k} + \sum_{k=7}^{32} N_k\delta^{i_k}\tau^{j_k}\exp\left(-\delta^{l_k}\right) \\ & + \sum_{k=33}^{36} N_k\delta^{i_k}\tau^{j_k}\exp\left(-\varphi_k(\delta-1)^2 - \beta_k(\tau-\gamma_k)^2\right)\end{aligned} \quad \text{(Nitrogen)} \tag{10}$$

$$\alpha^r(\delta,\tau) = \sum_{k=1}^{13} N_k\delta^{i_k}\tau^{j_k} + \sum_{k=14}^{32} N_k\delta^{i_k}\tau^{j_k}\exp\left(-\delta^{l_k}\right) \quad \text{(Oxygen)} \tag{11}$$

The parameters and coefficients for the nitrogen and oxygen in Eq. (9), (10) and (11) are found in the references [19, 20]. In Fig. 2, densities of the nitrogen and the oxygen at supercritical pressures of interest (100, 200, and 400 atm) predicted by the fundamental equation of state are compared with experiments.

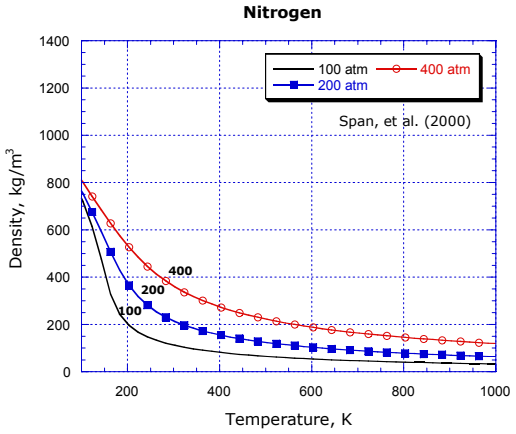

(a) Nitrogen

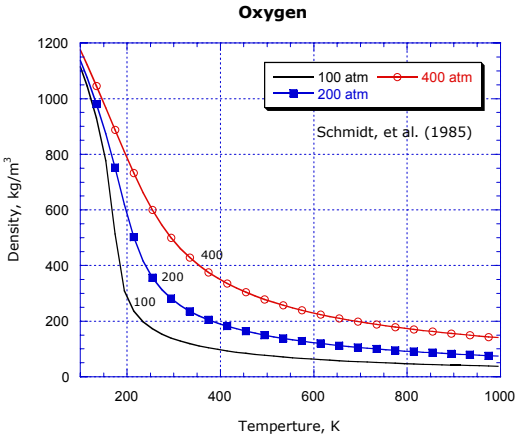

(b) Oxygen

Fig. 2. Density changes of nitrogen and oxygen as a function of temperature at supercritical pressures.

Here, coefficients and empirical data were taken from the results of Span, et al. [19] and Schmidt, et al. [20] for the nitrogen and the oxygen, respectively. For both the nitrogen and the oxygen, agreements in predicted and measured data at higher pressures are almost perfect.

A mixture model explicit in Helmholtz energy was first proposed by Lemmon [17] and Lemmon and Jacobsen [21]. This model is capable of predicting thermodynamic properties of mixtures containing nitrogen and oxygen within an estimated accuracy of available experimental data. The mixture Helmholtz energy is the sum of the ideal gas contribution, the compressibility (or real gas) contribution, and the contribution from mixing. The contribution from mixing is given by a single generalized equation in terms of independent variables (the density, temperature, and composition) [22]. The equation for the mixture Helmholtz energy used here is

$$a = a^{idmix} + a^{E} \tag{12}$$

The Helmholtz energy for an ideal mixture a^{idmix} is:

$$\frac{a^{idmix}}{RT} = \sum_{i=1}^{n} x_i \left[\alpha_i^0(\rho, T) + \alpha_i^r(\delta, \tau) + \ln x_i \right] \tag{13}$$

In Eq. (13), ρ and T are the mixture density and temperature, δ ($\equiv \rho/\rho_{red}$) and τ ($\equiv T_{red}/T$) are the reduced mixture density and temperature, n is the number of components in the mixture, α_i^0 is the ideal gas Helmholtz energy of component i, α_i^r is the residual Helmholtz energy of component i, and the x_i are the mole fractions of the mixture constituents. The contribution to the Helmholtz energy from mixing a^E in Eq. (12) is:

$$\frac{a^E}{RT} = \alpha^E(\delta, \tau, x) = \sum_{i=1}^{n-1} \sum_{j=i+1}^{n} x_i x_j F_{ij} \sum_{k=1}^{10} N_k \delta^{d_k} \tau^{t_k} \tag{14}$$

The parameters, coefficients and exponents in Eq. (13), (14) are found in the reference [22].

Property relations for pressure, compressibility factor, internal energy, enthalpy, isochoric heat capacity, and isobaric heat capacity are:

$$p = \rho RT \left[1 + \delta \left(\frac{\partial \alpha^r}{\partial \delta} \right) \right]_\tau \tag{15}$$

$$Z = \frac{p}{\rho RT} = 1 + \delta \left(\frac{\partial \alpha^r}{\partial \delta} \right)_\tau \tag{16}$$

$$\frac{h}{RT} = \tau \left[\left(\frac{\partial \alpha^0}{\partial \tau} \right)_\delta + \left(\frac{\partial \alpha^r}{\partial \tau} \right)_\delta \right] + 1 + \delta \left(\frac{\partial \alpha^r}{\partial \delta} \right)_\tau \tag{17}$$

$$\frac{C_v}{R} = -\tau^2 \left[\left(\frac{\partial^2 \alpha^0}{\partial \tau^2} \right)_\delta + \left(\frac{\partial^2 \alpha^r}{\partial \tau^2} \right)_\delta \right] \tag{18}$$

$$\frac{C_p}{R} = \frac{C_v}{R} + \frac{\left[1 + \delta \left(\frac{\partial \alpha^r}{\partial \delta} \right)_\tau - \delta\tau \left(\frac{\partial^2 \alpha^r}{\partial \delta \partial \tau} \right) \right]^2}{\left[1 + 2\delta \left(\frac{\partial \alpha^r}{\partial \delta} \right)_\tau + \delta^2 \left(\frac{\partial^2 \alpha^r}{\partial \delta^2} \right) \right]} \tag{19}$$

In these equations, the term α^0 is the contribution by the ideal gas,

$$\alpha^0 = \sum_{i=1}^{n} x_i \left[\frac{a_i^0(\rho,T)}{RT} + \ln x_i \right] \tag{20}$$

and the term α^r is the contribution from the residual Helmholtz energy of the pure fluids and from the Helmholtz energy contribution to mixing

$$\alpha^r = \alpha^E(\delta,\tau,x) + \sum_{i=1}^{n} x_i \frac{a_i^r(\delta,\tau)}{RT} \tag{21}$$

In subcritical conditions, droplet surface is distinctly distinguished from outer gas mixture so that droplet vaporization, deformation and breakup processes are controlled by convective effects of the gas stream since the liquids are much less mobile than the gases. In contrast, at supercritical states, the droplet becomes a puff of dense fluid and no distinct interfacial boundary can be identified. The droplet deformation and the diffusion process control the droplet breakup and the emission processes, and correct prediction of the phenomenon hinges on accurate calculation of transport properties of the mixture.

Transport properties of oxygen are calculated by a preliminary equation by Laesecke, A. et al. [23]. Temperature and density dependence on the viscosity is considered as the sum of two contributions: the viscosity in the dilute gas state, $\eta_0(T)$, which is only a function of temperature, and the excess or residual viscosity, $\Delta\eta(\rho)$, which is only density-dependent :

$$\eta(\rho,T) = \eta_0(T) + \Delta\eta(\rho) \tag{22}$$

Since oxygen is a small diatomic molecule, the temperature dependence on its viscosity in the dilute gas state or zero-density limit can be well represented by a kinetic theory. However, particular density dependence on $\Delta\eta(\rho)$ cannot be taken for granted for all substances universally. Before a correlation is attempted, the functional density dependence has to be provided.

Calculation scheme for thermal conductivity is analogous to that of viscosity. The temperature dependence on the total thermal conductivity $\lambda(\rho,T)$ results from the thermal conductivity in the zero-density limit $\lambda_0(T)$ while the density dependence is incorporated in the residual contribution $\Delta\lambda(\rho)$. The third term $\Delta\lambda_c(\rho,T)$ is required to represent the critical enhancement,

$$\lambda(\rho,T) = \lambda_0(T) + \Delta\lambda(\rho) + \Delta\lambda_c(\rho,T) \tag{23}$$

Since the residual thermal conductivity, $\Delta\lambda(\rho)$, is typically less density-dependent than the residual viscosity, it can be represented by polynomial expressions. And the critical enhancement of the thermal conductivity, $\Delta\lambda_c(\rho,T)$, can be expressed with some kinetic theory and correlations.

Viscosity and thermal conductivity of nitrogen are calculated by preliminary equations by Lemmon et al [21]. The transport properties of nitrogen, oxygen and mixture are calculated with ECS type of mixing rule. Relevant information can be found in the references: Klein et al. [24] and McLinden et al. [25].

Due to the lack of a formal theory or even a theoretically based correlation, estimation of the binary mass diffusivity for a gaseous mixture at high density represents a more challenging task than evaluating other transport properties,. For a multicomponent system, effective diffusion coefficient D_{im} for each species i can be related to the binary diffusion coefficients through the following formula:

$$D_{im} = \frac{(1-x_i)}{\sum_{j\neq i}^{N} \left(x_j / D_{ij} \right)} \qquad i = 1,\ldots,N \tag{24}$$

Here, x_i is the mole fraction of species i. The binary mass diffusivity D_{ij} for the gas phase is obtained by using the corresponding-state model proposed by Takahasi [26]. Property evaluation is divided into two parts. First, the binary mass diffusivity of a dilute mixture is obtained from the Chapman-Enskog theory in conjunction with the Lennard-Jones intermolecular potential-energy function [27]. Values obtained for the dilute mixture is then corrected with a pressure correction factor, which is expressed in a generalized chart in terms of reduced temperature and pressure. This scheme appears to be the most complete to date, and has demonstrated moderate success in the limited number of tests conducted.

3. Results and discussion

At subcritical thermodynamic state, mass diffusivity and enthalpy of vaporization which are inversely proportional to ambient pressure determine the characteristics of stagnant droplet evaporation. In convective environment, the gas flow expedites droplet vaporization and breakup processes because convective mass and heat transfers are superior to diffusive transports. On the other hand, in a supercritical condi-

tion, the droplet becomes a puff of dense fluid with indistinct interfacial droplet boundary. External gas flow transfers momentum directly to the puff-state droplet and deformation takes place because the liquid-like gas has less resistance to driving gas stream than the liquid. The convection effects diminish, and both droplet emission and secondary breakup depend on the extents of mass diffusivity and droplet deformation which are strong function of ambient pressure.

Experiments for supercritical droplet and spray dynamics are numerous, but few records exist for a single supercritical droplet because of the experimental difficulties. Therefore, a parametric investigation on the effects of the ambient pressure and gas flow velocity is made to elucidate the peculiarities of a supercritical droplet emission in cross flows. For a liquid oxygen droplet suddenly exposed to a supercritical nitrogen stream, effects of ambient gas pressure and velocity on the supercritical emission and droplet dynamics are examined. Initial droplet temperature and diameter are commonly $100\,K$ and $100\,\mu m$, respectively, and the ambient nitrogen temperature is $1000\,K$.

Fig. 3 shows the structured grid system composed of a total of 304,401 (301X101) grid points. In order to resolve small scale phenomena such as inter-phase dynamics, droplet emission and micro-macroscopic diffusion, the computational domain is finely segmented with the grid size determined after the grid sensitivity analysis.

At the conditions prevalent in high-pressure vaporization, thermophysical properties strongly depend on pressure, temperature, and composition. More elaborated studies revealed that droplet combustion is more transient, not being ruled by D^2 law, and droplet lifetime is reduced as the ambient pressure increases. Moreover, convective transport is greatly activated with the increase in droplet Reynolds number as a function of relative velocity. Evidently, the supercriticality and interactive dynamics controls the droplet dynamics at high pressures. To this end, effects of ambient flow parameters (convective velocity and ambient pressure) on droplet behavior and associated multi-species transport are investigated. The test matrix is composed of the elements of three ambient pressures of 100, 200, and 400 atm in combination with four flow velocities 3, 7, 11, and 15 m/s. Since the largest drop Reynolds number is slightly over 4,000 in the range of examined gas velocities, flows are laminar in place on the droplet surface and no turbulence effect is taken into consideration.

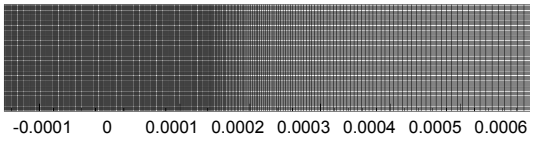

Fig. 3. The structured grid system with 304,401 (301x101) grid points.

Critical temperature and pressure of oxygen are $54.361\,K$ and $49.771\,atm$, respectively. Therefore, the oxygen droplet of temperature of 100 K and pressures greater than 100 atm is at its supercritical state immediately after its introduction into the gas stream, and thus the droplet may be treated as a dense liquid-like gas (puff). Enthalpy of vaporization and surface tension vanish, and the temperature and density as well as their spatial gradients vary smoothly on the entire domain of interest. The subsequent droplet emission process becomes diffusion-convection controlled, and influence of interfacial thermodynamics becomes minimal.

Unlike typical viscous dissipation at rigid wall surface, the dissipation between gas and puff in the case of supercritical droplet is significant since the droplet is accelerated and settles down to the gas motion with reduced relative velocity. Though the total pressure is less dissipated, droplet is deformed mainly due to uneven local pressures and lack of surface tension. Under all thermal and flow conditions examined, the critical boundary moves faster into the droplet interior in the rear of droplet than in the front. It may result from the deformation of droplet with increasing shear stress on top of droplet rather than the promotion of convective transport due to the recirculation in the rear of droplet. Strong momentum carried and transferred by the nitrogen stream impinging on the front surface results in positive pressure drag, which exerts compressing force on the droplet surface. Consequently, the droplet is compressed and deformed into a bulged shape.

Several snapshot pictures of the diffusing oxygen droplet are presented in Fig. 4 through 10 according to aforementioned initial conditions in the test matrix. In every column, ten frames of isotherm and iso-concentration contours of the oxygen are presented which correspond to a time sequence from 10 to 100 microseconds. Fig. 4 presents temperature and O_2 concentration contours of evolving oxygen droplet in supercritical nitrogen flow at pressure of 100 atm, and velocity of 3 m/s. Soon after sudden introduction of a

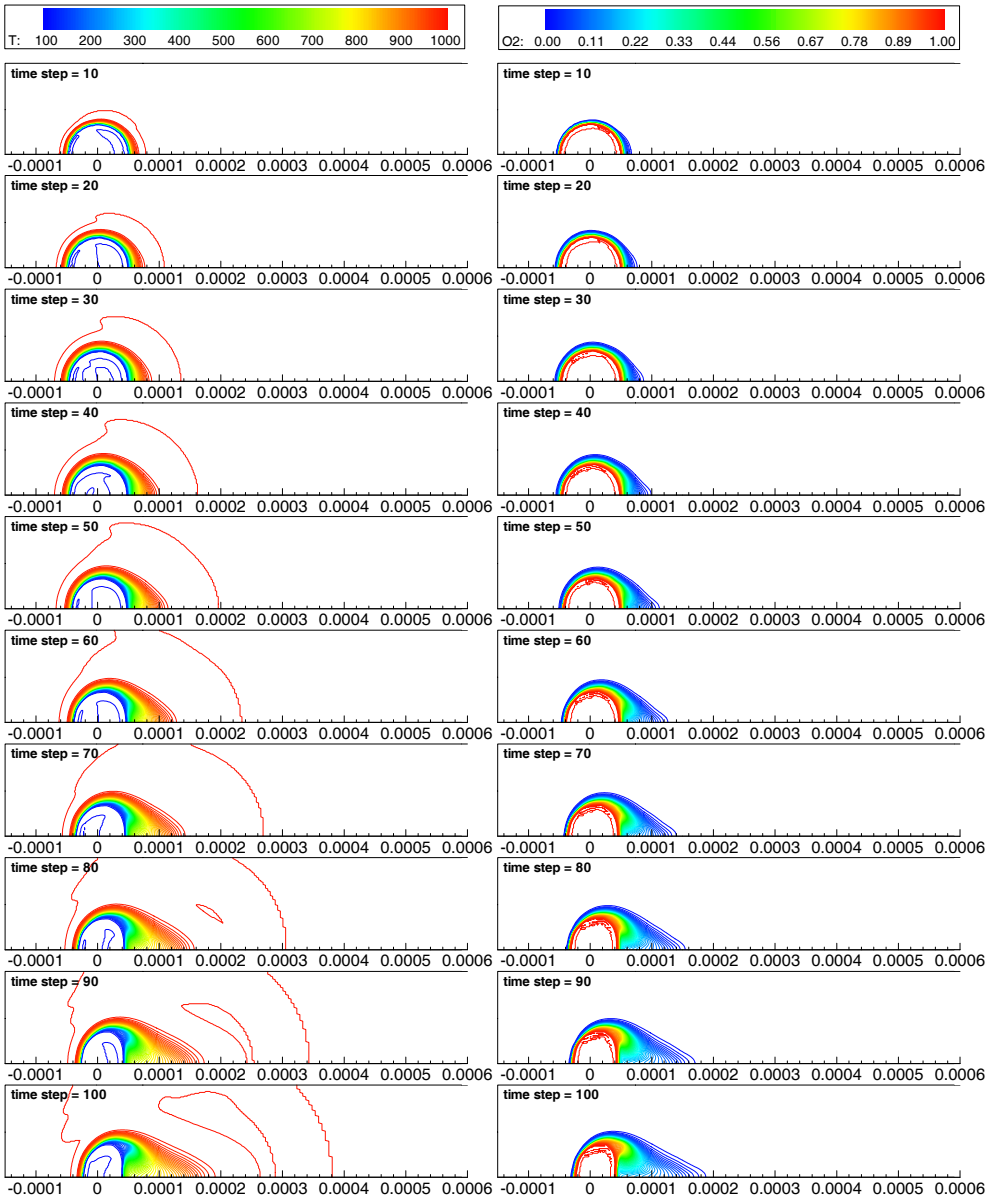

(a) Isothermal lines (b) Iso-concentration lines of O_2

Fig. 4. Evolution of supercritical oxygen droplet in nitrogen cross-flow (p=100 atm, U_∞=3m/s).

stagnant droplet (3 m/s relative velocity) into the nitrogen gas stream, the flow conforms to make a boundary layer near the surface. The convective stream is from left to right, and a stagnation point at which the diffusion velocity of the supercritical fluid emitting from the droplet is counter-balanced by the convection velocity of sweeping nitrogen gas flow streaming downstream forms immediately upstream of the droplet. Diffused oxygen is not stretched upstream or piled up in the vicinity of stagnation point, and the excessive oxygen gas in this zone is swept away along the droplet surface while it forms a boundary layer of gaseous oxygen of reduced concentration. The boundary layer above the stagnant point is not altered by the oxygen emission, but it gradually grows as the flow proceeds downstream along the

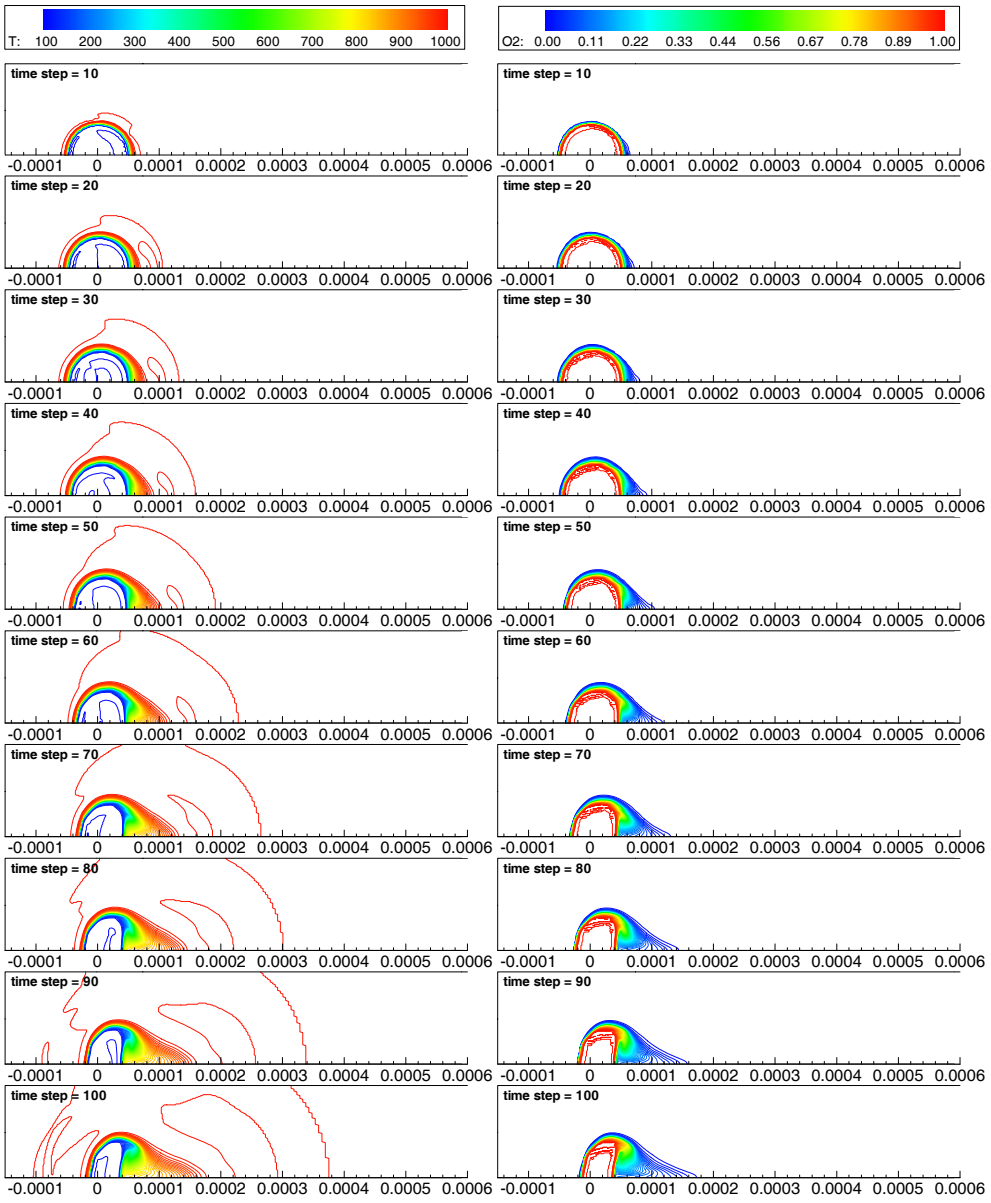

(a) Isothermal lines (b) Iso-concentration lines of O_2

Fig. 5. Evolution of supercritical oxygen droplet in nitrogen cross-flow (p=200 atm, U_∞=3m/s).

droplet surface. Excessive oxygen mass transported from the droplet frontal surface, successive mass diffused from the lateral surface, and spherical droplet configuration are primary causes for the boundary-lay growing.

The effect of the ambient pressure and velocity to the deformation and emission of an isolated supercritical droplet is complex and interactive. To see the effect of ambient pressure at a fixed gas flow velocity, the test cases are categorized into two groups of carrier-gas different velocities of 3 m/s and 7 m/s, respectively. At every flow velocity, the ambient pressure is varied from 100 to 400 atm.

Figs. 4, 5 and 7 show an evolving droplet at ambient pressure of 100, 200 and 400 atm, respectively, with a fixed nitrogen velocity at 3m/s. Effect

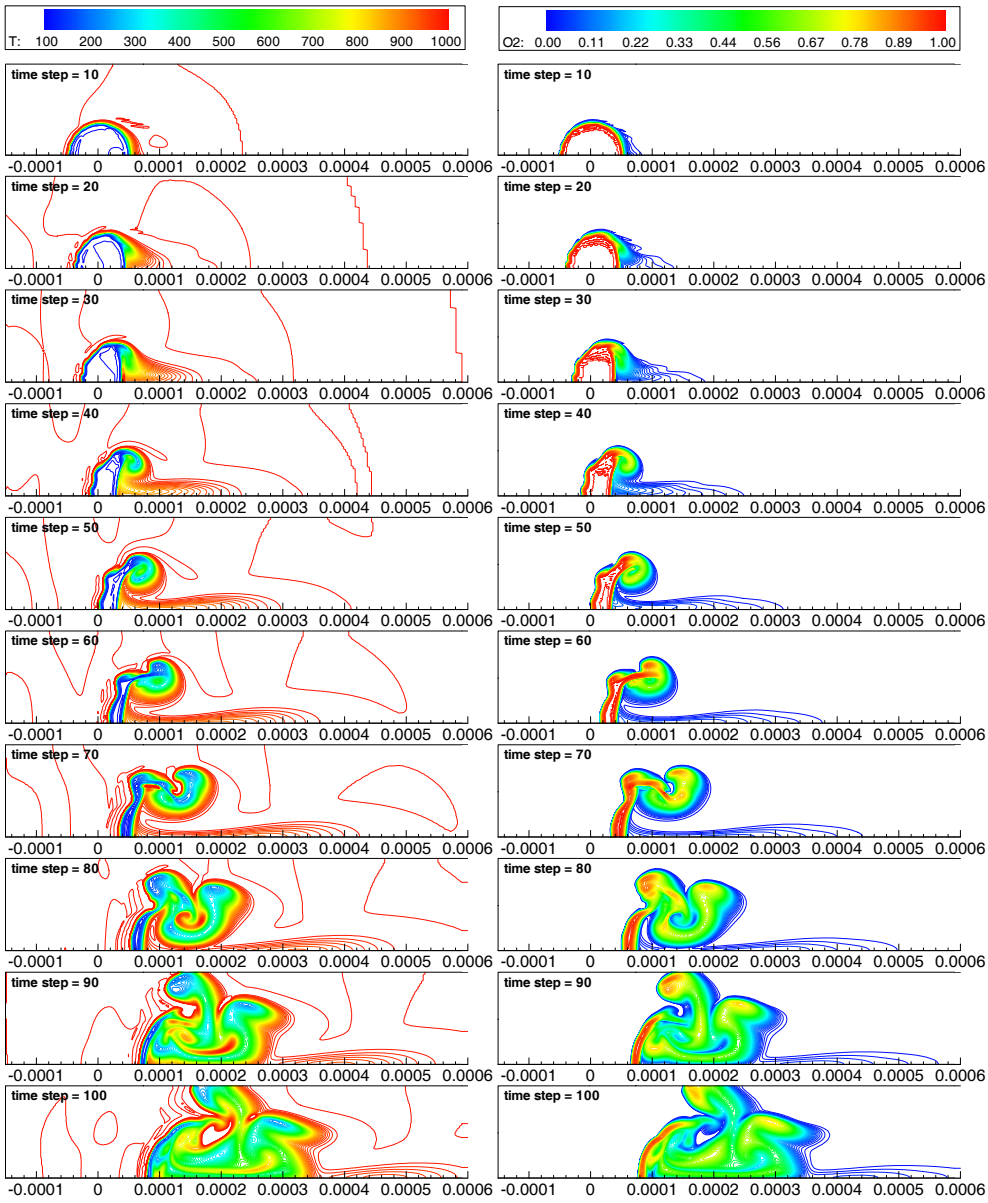

(a) Isothermal lines (b) Iso-concentration lines of O_2

Fig. 6. Evolution of supercritical oxygen droplet in nitrogen cross-flow (p=200 atm, U_∞=7m/s).

of ambient pressure on droplet dynamics in weakly convective flow condition can be seen by a direct comparison. Droplet deformation is further expedited at higher ambient pressure. Since the nitrogen stream carries strong momentum and thus causes larger pressure difference between the front and the rear surface of the droplet. Droplet lifetime is reduced with increasing in ambient pressure since the droplet bulges out with increasing in the surface area, and the mass transport is proportionally augmented even with the same convection condition.

Figs. 6 and 8 show droplet evolution at ambient pressure of 200 atm and 400 atm when the gas velocity is 7 m/s. Effects of ambient pressure on the droplet are also observed, its profile is significantly altered at such increased gas velocity. The most

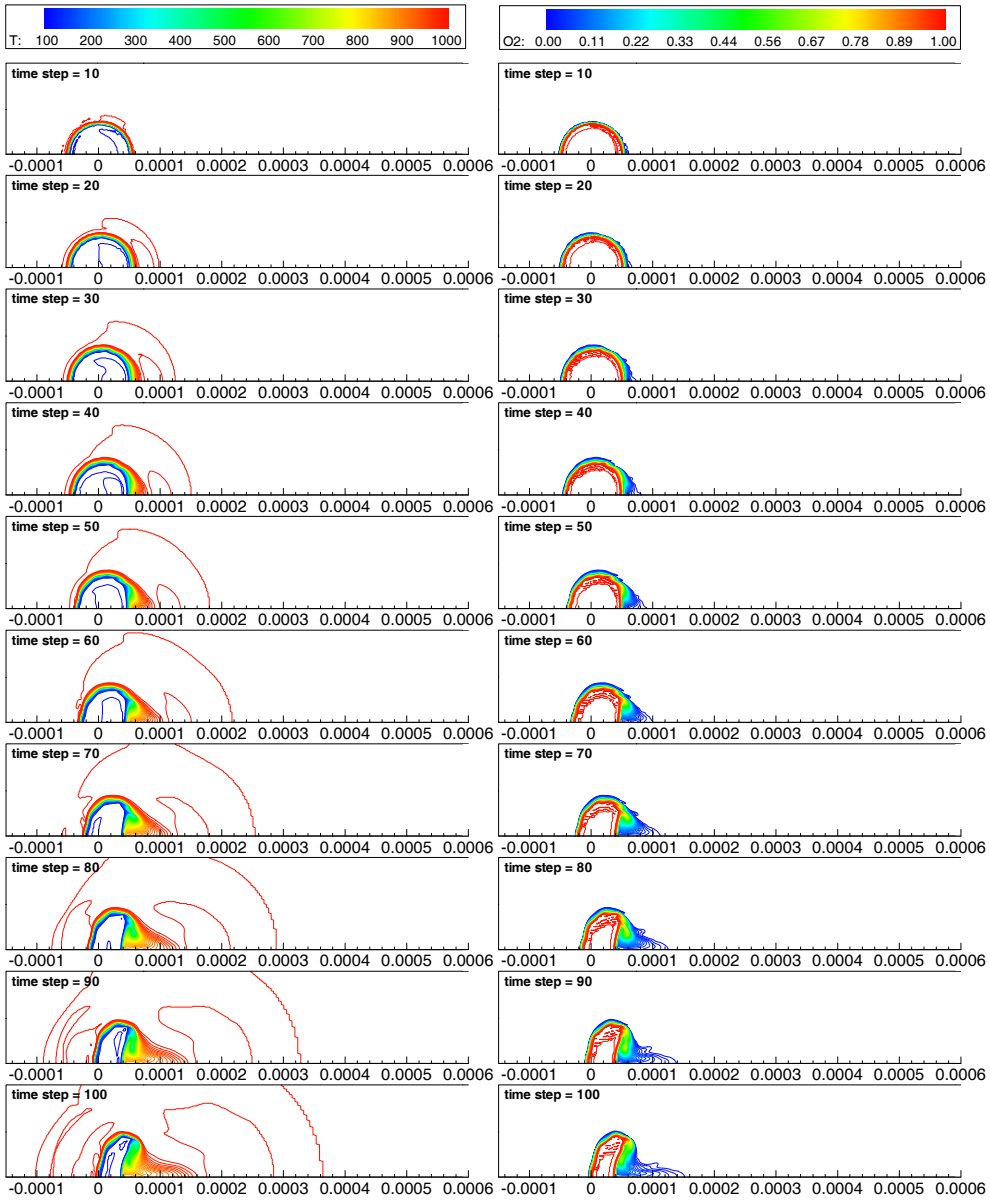

(a) Isothermal lines (b) Iso-concentration lines of O_2

Fig. 7. Evolution of supercritical oxygen droplet in nitrogen cross-flow (p=400 atm, U_∞=3m/s).

distinct difference caused by the convection is less active droplet deformation. Secondary breakup is hindered by reduced diffusivity at higher ambient pressure. These results reveal that there is no similarity in the characteristics of supercritical droplet emission and deformation with regard to the ambient pressure since the phenomenon strongly depend on the convection characteristics as well.

Ambient pressure and gas flow velocity for optimum supercritical droplet emission and mixing depend on the system requirements or demands. In Fig. 6, overall feature of evolving droplet is significantly different from the previous cases (Figs. 4 and 7) and exhibits several distinct flow modes such as deformation, viscous stripping, and secondary breakup and more. The droplet lifetime generally decreases with

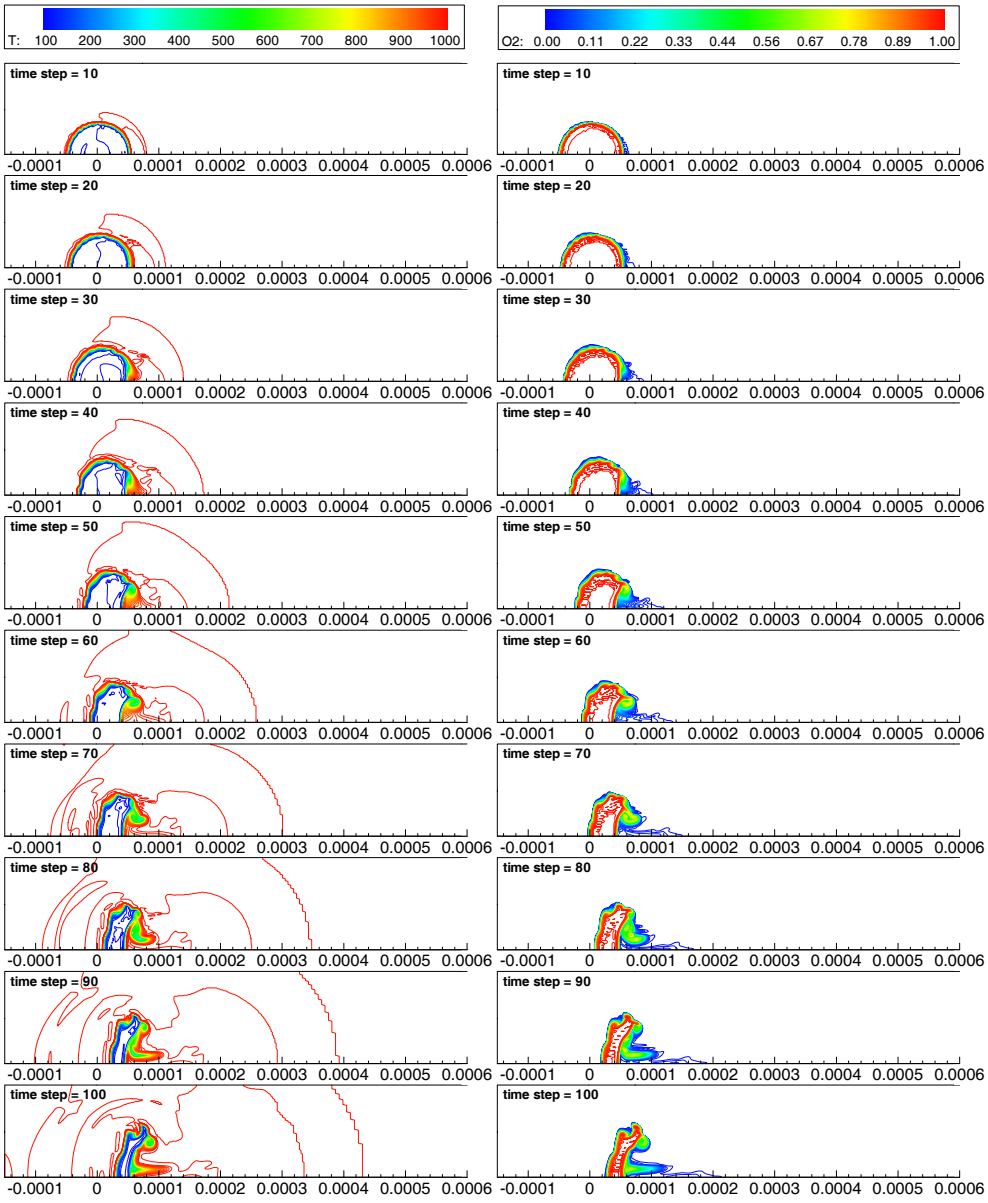

(a) Isothermal lines (b) Iso-concentration lines of O_2

Fig. 8. Evolution of Supercritical Oxygen Droplet in Nitrogen Cross-Flow (p=400 atm, U_∞=7m/s).

increasing in gas Reynolds number since augmented momentum transfer in the boundary layer enhances the convective heat transfer into droplet and correspondingly emission.

When the gas stream of strong momentum is hindered by the presence of the droplet, aerodynamic forces acting on the droplet surface result in the secondary flows. Fast vortex generation caused by the velocity difference between the droplet core and ambient gas flow promotes the formation of an attached eddy behind the droplet. The droplet aspect ratio increases with time and flattened edge of the droplet may enhance the strength of recirculating eddies and as such increases the viscous shear stress dramatically. As a result, a thin sheet of dense oxygen may be stripped from the edge of the droplet and swept by

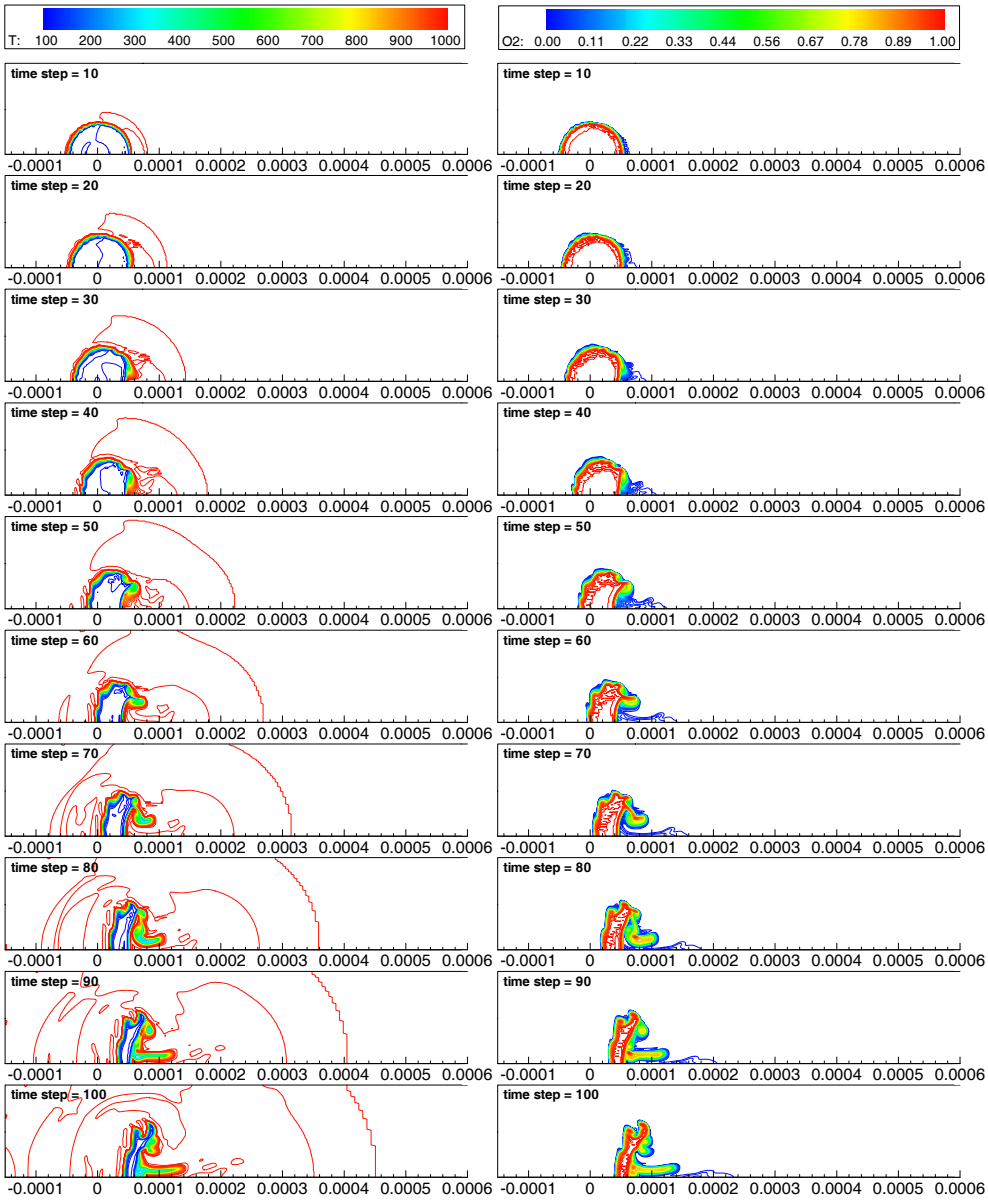

(a) Isothermal lines (b) Iso-concentration lines of O_2

Fig. 9. Evolution of supercritical oxygen droplet in nitrogen cross-flow (p=400 atm, U_∞=11m/s).

shear flows to downstream. In Fig. 6, the secondary breakup occurs during 30 to 60 microseconds. Meanwhile, the free stream exerts dynamic loading continuously to the front surface to induce the subsequent breakup ($50 \sim 60\,\mu\text{sec}$). As a result, the droplet deforms and extends in the direction normal to the external flow. The flattened edge, as shown at $t = 60\,\mu\text{sec}$, then turns to the streamwise direction, stretches downstream, and increases the extent of mixing. The mixing quality determined by the extent of the momentum transfer from the ambient flow progressively improves. At $t = 80\,\mu\text{sec}$, the eddies of gaseous oxygen are detached from the growing skirt due to the local flow motion and volume dilution. The stripped oxygen, partly entrained by the recirculating flow, further bends toward the rear part of the

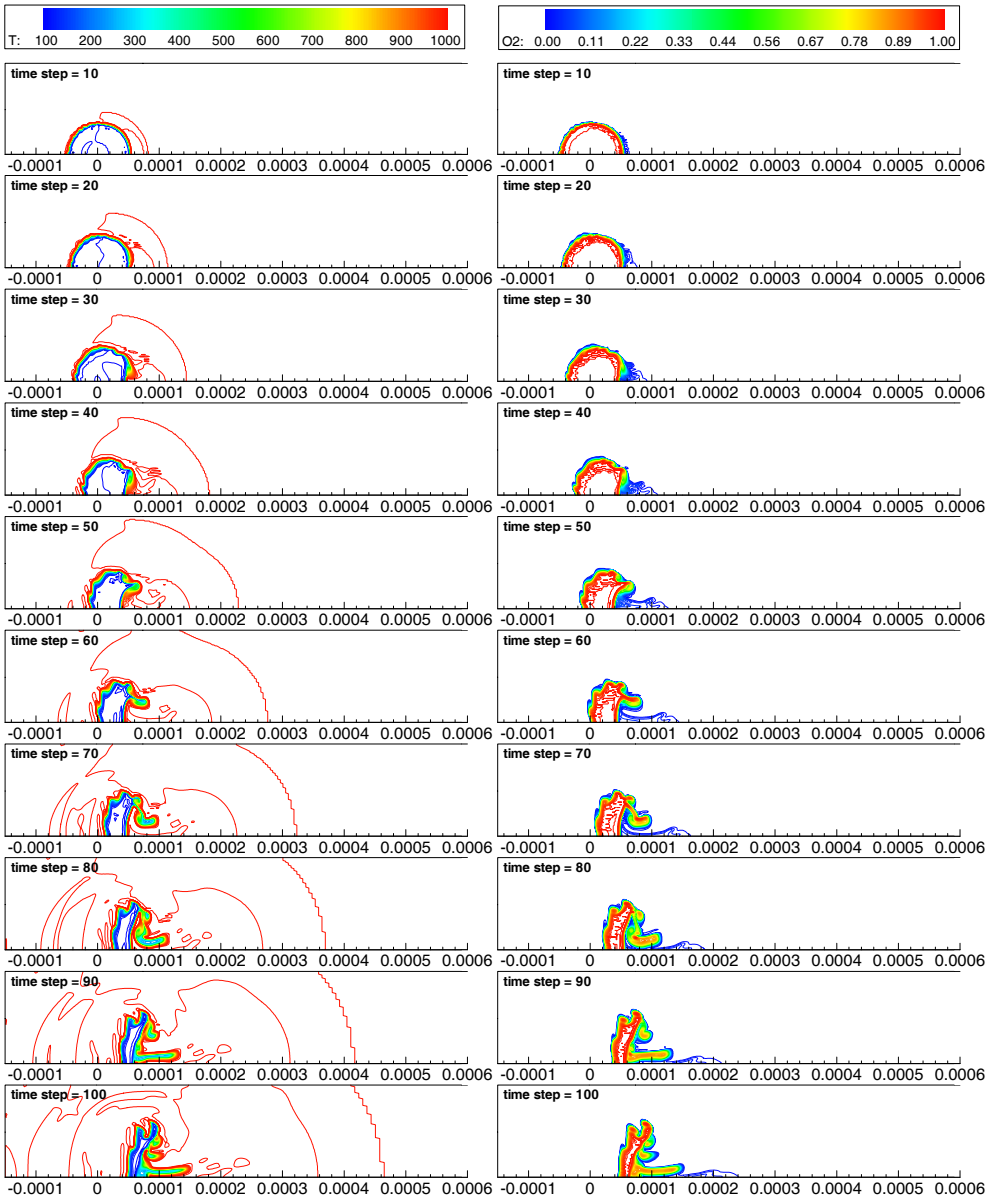

(a) Isothermal lines (b) Iso-concentration lines of O_2

Fig. 10. Evolution of supercritical oxygen droplet in nitrogen cross-flow (p=400 atm, U_∞=15m/s).

droplet. It carries the momentum from the attached eddy and consequently causes the droplet to deform into a parachute or crescent shape.

Evolutions of emitted droplet at high pressure (400 atm) are presented in Fig. 7 through 10 in terms of gas velocities. Increasing the momentum carried by the ambient flow substantially expedites the dynamic deformation of the droplet. As the velocity of gas stream increases, the droplet aspect ratio and its acceleration gradually increase. Wiggles in front of the droplet are growing in wavelike fashion and separate into two fragments; one into a secondary breakup, the other into a subsequent breakup. It is commonly observed that the stagnation point proceeds further downstream as the gas velocity increases regardless of ambient pressure (Figs. 5 through 9)

At lower pressure of 100 atm, the diffusion mode controls deforming and emitting the droplet and the stagnant point is shifted downstream due to reduced mass transport. Paralleled with the droplet deformation drag force on the droplet gets stronger and accelerates the droplet.

Since turbulent diffusion and mixing are not available, molecular diffusion is the only transport mode for the component mixing between gas flow and puff droplet. As a result, convection and diffusion velocities in conjunction with the droplet deformation and fluid dynamical interaction determine the mixing quality. In Fig. 6, at intermediate pressure of 200 atm and velocity of 7 m/s, the occurrence of strong eddy cascade in which the eddy breaks down into three vortexes is clearly observed. Unlike low-pressure models in which the large shear stress at the gas-liquid interface induces internal flow circulation in the droplet core [28], the occurrence of recirculation at the droplet interior was not perceptible at all pressures and velocities examined. Diminishing surface tension of puff state fluid at supercritical condition may be a possible cause. In addition, the droplet surface regresses so rapidly that relaxation time to sustain recirculation within the droplet is insufficient. Rapid deformation of a droplet prevents the occurrence of the recirculation at the droplet interior.

4. Concluding remarks

Dynamics and emission of a supercritical droplet in a crossing gas stream are numerically investigated. Evolution of cryogenic liquid-like oxygen droplet in the nitrogen gas stream with droplet Reynolds number less than 4500 is parametrically examined in terms of gas pressure and velocity.

Supercriticality and relative fluid motions control the droplet dynamics at high pressures. Uneven local surface pressures deform the droplet into a bulged shape and the critical boundary moves faster into the droplet interior while an occurrence of flow recirculation inside the droplet is hindered. Mixing of emitted oxygen with the nitrogen gases depends on the convection and diffusion velocities in conjunction with corresponding droplet deformation and flow interaction.

Both the modes of diffusion and convection are essential to the transports at low pressures. In a weakly convective environment with the carrier-gas velocity of 3 m/s, relative flow motion causes secondary breakup and vertical fluid motion. The droplet lifetime is reduced with increasing in the ambient pressure. At higher ambient pressures, the droplet dynamics become convection-controlled with increasing in the gas velocities while the secondary breakup is hindered by reduced diffusivity of the oxygen at high pressures. No obvious similarity in the characteristics of supercritical droplet dynamics and emission is observed with regard to the ambient pressure and velocity. The present rigorous study on the supercritical droplet emission and dynamics is expected to provide fundamentals essential to designing and enhancing industrial high-pressure combustion.

References

[1] R. Lide David, CRC Handbook of Chemistry and Physics, 68th ed., CRC Press Inc., (1987).

[2] S. D. Givler and J. Abraham, Supercritical Droplet Vaporization and Combustion Studies, Progress in Energy and combustion Science 22, (1996), 1-28.

[3] P. R. Wieber, Calculated Temperature Histories of Vaporizing Droplets to Critical Point, AIAA Journal 1, (1963), 2764-2770.

[4] J. A. Manrique and G. L. Borman, Calculations of Steady State Droplet Vaporization at High Ambient Pressures, Intl. J. of Heat Mass Transfer 12, (1969), 1081-1095.

[5] G. L. Hubbard, V. E. Denny and A. F. Mills, Droplet Evaporation: Effects of Transitions and Variable Properties, Intl. J. of Heat Mass Transfer 18, (1975), 1003-1008.

[6] R. L. Matlosz, S. Leipziger and T. P. Torda, Investigation of Liquid Droplet Evaporation in a High Temperature and High Pressure Environment, Intl. J. of Heat Mass Transfer 15, (1972), 831-852.

[7] K. C. Hsieh, J. S. Shuen and V. Yang, Droplet Vaporization in High-Pressure Environments. I: Near Critical Conditions, Comb. Sci. and Tech. 76, (1991), 111-132.

[8] J. S. Shuen, V. Yang and C. C. Hsiao, Combustion of Liquid-Fuel Droplets in Supercritical Conditions, Combustion and Flame 89, (1992), 299.

[9] L. P. Combs, Calculated Propellant Droplet Heating under F-1 Combustion Chamber Conditions, Rocketdyne RR 64-25, (1964).

[10] J. C. Oefelein and S. K. Aggarwal, Toward a unified high-pressure drop model for spray simulations, Center for Turbulence Research, Proceedings of the Summer Program, (2000), 193-205.

[11] J. Sato, M. Tsue, M. Niwa and M. Kono, Effects of natural convection on high-pressure droplet com-

bustion, Comb. and Flame 82, (1990), 142-150.
[12] C. K. Law, Recent Advances in Droplet Vaporization and combustion, Progress in Energy and Combustion Science 8, (1982), 171-201.
[13] J. P. Withington, A Time Accurate Numerical Method for Chemically Reacting Flows at All Mach Numbers, Ph.D. Thesis, The Pennsylvania State University, University Park, Pennsylvania, (1992).
[14] G. C. Hsiao, Supercritical Droplet Vaporization and Combustion in Quiescent and Forced-Convective Environments, Ph.D. thesis, The Pennsylvania State University, University Park, PA, (1995).
[15] C. L. Merkle and Y. H. Choi, Computation of Low-Speed Flow with Heat Addition, AIAA Journal 23, (1987), 831-838.
[16] J. S. Shuen, K.-H. Chen and Y. Choi, A Coupled Implicit Method for Chemical Non-equilibrium Flows at All Speeds, J. of Computational Physics 106, (1992), 306-318.
[17] E. W. Lemmon, A Generalized Model for the Prediction of the Thermodynamic Properties of Mixtures Including Vapor-Liquid Equilibrium, Ph.D. Thesis, University of Idaho, (1996).
[18] R. B. Stewart and R. T. Jacobsen, Thermodynamic Properties of Argon from the Triple Point to 1200 K at Pressures to 1000 MPa, J. Phys. Chem. Ref. Data 18(2), (1989), 639-798.
[19] R. Span, E. W. Lemmon, R. T. Jacobsen, W. Wagner and A. Yokozeki, A Reference Equation of State for the Thermodynamic Properties of Nitrogen for Temperature from 63.151 to 1000 K and Pressures to 2200 MPa, J. Phys. Chem. Ref. Data 29(6), (2000).
[20] R. Schmidt and W. Wagner, A New Form of the Equation of State for Pure Substances and Its Application to Oxygen, Fluid Phase Equilibria 19, (1985), 175-200.
[21] E. W. Lemmon and R. T. Jacobsen, A Generalized Model for the Thermodynamic Properties of Mixtures, Intl. J. of Thermophysics 20(3), (1999), 825.
[22] E. W. Lemmon, R. T. Jacobsen, S. G. Penoncello and D. G. Friend, Thermodynamic Properties of Air and Mixtures of Nitrogen, Argon, and Oxygen From 60 to 2000 K at Pressures to 2000 MPa, J. Phys. Chem. Ref. Data 29(3), (2000).
[23] A. Laesecke, R. Krauss, K. Stephan and W. Wagner, Transport Properties of Fluid Oxygen, J. Phys. Chem. Ref. Data 19(5), (1990), 1089.
[24] S. A. Klein, M. O. McLinden and A. Laesecke, An Improved Extended Corresponding States Method for Estimation of Viscosity of Pure Refrigerants and Mixtures, Int. J. Refrig. 20(3), (1997), 208-217.
[25] M. O. McLinden, S. A. Klein and R. A. Perkins, An Extended Corresponding States Model for the Thermal Conductivity of Refrigerants and Refrigerant Mixtures, Int. J. Refrig. 2, (2000), 43-63.
[26] S. Takahashi, Preparation of a Generalized Chart for the Diffusion Coefficients of Gases at High Pressures, J. of Chemical Engineering (Japan) 7, (1974), 417-420.
[27] C. R. Wilke and C. Y. Lee, Estimation of Diffusion Coefficients for Gases and Vapors, Industrial Engineering Chemistry 47, (1955), 1253-1257.
[28] S. Prakash and W. A. Sirignano, Liquid Fuel Droplet Heating with Internal Circulation, Int. J. Heat Mass Transfer 21, (1978), 885.
[29] E. R. Cohen and B. N. Taylor, The 1986 CODATA recommended values of the fundamental physical constants, J. Phys. Chem. Ref. Data, 17, (1988), 1795-1803.
[30] G. C. Maitland, M. Mustafa and W. A. Wakeham, Thermal-conductivity of Polyatomic Gases at Low Density, J. Chem. Soc. Faraday Trans. 79, (1983), 163-172.
[31] R. C. Reid, J. M. Prausnitz and B. E. Poling, The Properties of Gases and Liquids, McGraw-Hill, Inc., (1988).